The Astrophysical Journal Letters, 949:L19 (6pp), 2023 June 1 https://doi.org/10.3847/2041-8213/acd4c2


# Compressible Turbulence in the Near-Sun Solar Wind: Parker Solar Probe's First Eight Perihelia

Manuel Enrique Cuesta[1], Rohit Chhiber[1,2], Xiangrong Fu[3,4], Senbei Du[4], Yan Yang[1], Francesco Pecora[1], William H. Matthaeus[1], Hui Li[4], John Steinberg[4], Fan Guo[4], Zhaoming Gan[3,4], Emma Conrad[4], and Diana Swanson[4,5]
[1] Department of Physics and Astronomy, Bartol Research Institute, University of Delaware, Newark, DE 19716, USA; mecuesta@udel.edu
[2] NASA Goddard Space Flight Center, Greenbelt, MD 20771, USA
[3] New Mexico Consortium, Los Alamos, NM 87544, USA
[4] Los Alamos National Laboratory, Los Alamos, NM 87545, USA
[5] University of New Hampshire, Durham, NH 03824, USA
*Received 2023 March 10; revised 2023 May 5; accepted 2023 May 9; published 2023 May 26*

## Abstract

Many questions remain about the compressibility of solar wind turbulence with respect to its origins and properties. Low plasma beta (ratio of thermal to magnetic pressure) environments allow for the easier generation of compressible turbulence, enabling study of the relationship between density fluctuations and turbulent Mach number. Utilizing Parker Solar Probe plasma data, we examine the normalized proton density fluctuations $\langle \delta n_p^2 \rangle^{1/2} / \langle n_p \rangle = \delta n_{p_{\rm rms}} / \langle n_p \rangle$ as a function of turbulent Mach number $M_t$ conditioned on plasma beta and cross helicity. With consideration of statistical error in the parameters computed from in situ data, we find a general result that $\delta n_{p_{\rm rms}} / \langle n_p \rangle \sim M_t^{1.18 \pm 0.04}$, consistent with both linear-wave theory and nearly incompressible turbulence in an inhomogeneous background field. We compare observational results conditioned on plasma beta and cross helicity with 3D magnetohydrodynamic simulations and observe rather significant similarities with respect to how those parameters affect the proportionality between density fluctuations and turbulent Mach number. This study further investigates the complexity of compressible turbulence as viewed by the density scaling relationship and may help better understand the compressible environment of the near-Sun solar wind.

*Unified Astronomy Thesaurus concepts:* Interplanetary turbulence (830); Plasma physics (2089); Space plasmas (1544)

## 1. Introduction

Density fluctuations persist on average at a low level of about 10% in the solar wind inertial range and over a wide range of heliocentric distances (Roberts et al. 1987b). The properties and origins of this compressible component of turbulence are still unclear. Density fluctuations are generated from a nonzero divergence of the velocity field; however, when available, the regime of low plasma beta $\beta$ (ratio of thermal to magnetic pressure) is a signature for an easier generation of compressible turbulence (Roberts et al. 1987a, 1987b; Grappin et al. 1990; Roberts et al. 1990; Bavassano & Bruno 1995; Malara et al. 1996), a consequence of the plasma being dragged and compressed by the dominant magnetic pressure, warranting a more detailed investigation. Such is the case in regions near recent Parker Solar Probe (PSP) perihelia due to the presence of a large (dominantly radial) magnetic field (Kasper et al. 2021) and the orbital approach to the coronal plasma, presumably of lower $\beta$ (e.g., Chhiber et al. 2019).

The coexistence of compressive and incompressive fluctuations in magnetohydrodynamic (MHD) turbulence has been observed in the solar wind, for example, by comparing spectra of density and magnetic field fluctuations, which have a similar power-law nature (Montgomery et al. 1987; Klein et al. 1993). Theories involving small-amplitude and slow-timescale compressive fluctuations have been used to expose the roles of Alfvén waves, pressure balances, and compressive waves in turbulent plasmas. Formally this involves an expansion of the compressible MHD equations about an incompressible state, based on small turbulent Mach numbers ($M_t$). This approach enables solutions characteristic of small-amplitude density fluctuations occurring at slow timescales (Matthaeus & Brown 1988; Matthaeus et al. 1991), namely, nearly incompressible (NI) theory. For a homogeneous background field, NI theory predicts that the rms density fluctuations scale with $M_t^2$. This theory is derived most directly when plasma beta is large, i.e., the sound speed is greater than the Alfvén speed ($c_s > V_{\rm A}$), which is typically not the case for heliocentric distances $R < 0.30$ au. However, large $V_{\rm A}$ need not invalidate NI dynamics if the associated wave frequencies $\boldsymbol{k} \cdot \boldsymbol{V}_{\rm A}$ remain small ($kV_{\rm A} \ll 1$) due to spectral (wavevector $\boldsymbol{k}$) anisotropy. Indeed, extensions of the theory to arbitrary plasma beta have also been presented, and these explicitly account for anisotropy relative to the mean magnetic field (Zank et al. 1990; Bayly et al. 1992; Zank & Matthaeus 1992, 1993). These extensions preserve the $M_t^2$ scaling in general.

Further generalizations of NI theory treat the case of an inhomogeneous background field and are perhaps most relevant to the solar wind; these theories predict a linear scaling of rms fluctuation strength with $M_t$ (Bhattacharjee et al. 1998; Hunana & Zank 2010; Zank et al. 2017; Adhikari et al. 2020a; Zank et al. 2021), a result also expected from a linearized analysis of the MHD equations (Cho & Lazarian 2003). The density scaling has been shown to also depend on $\beta$ (Cho & Lazarian 2003).

The turbulent Mach number $M_t \equiv \langle (\delta v)^2 \rangle^{1/2} / c_s$ is a key parameter that measures the compressibility of the turbulence, where $\langle (\delta v)^2 \rangle^{1/2} = \delta v_{\rm rms}$ is the rms of the velocity fluctuations, $\langle \cdot \rangle$ represents a suitable averaging operator, and $c_s$ is the ion sound speed. Equivalently,

$$M_t = \frac{\delta v_{\rm rms}}{V_{\rm A}} \sqrt{\frac{2}{\beta_p \gamma}} \tag{1}$$

can be written by making substitutions in favor of the Alfvén speed $V_{\rm A}$ with $c_s = \sqrt{\gamma k_B T / m_p}$, $\beta_p = 8\pi n_p k_B T / B^2$, and $V_{\rm A} = B/\sqrt{4\pi n_p m_p}$, where $\gamma$ is the polytropic index, $k_B$ is the Boltzmann constant, $T = T_p = T_e$ is the plasma temperature for protons and electrons, $m_p$ is the proton mass, $\beta_p$ is the ratio of thermal to magnetic pressure for protons, $n_p$ is the proton density, and $B$ is the magnetic field magnitude.

The purpose of this study is to further examine the relationship between density fluctuations and $M_t$. To better understand the nature of compressible MHD turbulence, many numerical simulations have been employed (Cho & Lazarian 2003; Kowal et al. 2007; Yang et al. 2016, 2017, 2019; Shoda et al. 2019; Makwana & Yan 2020; Yang et al. 2021; Fu et al. 2022; Gan et al. 2022). From a wave perspective, compressible MHD turbulence involves the nonlinear interactions between three distinct MHD modes: Alfvén, fast, and slow modes. Perpendicular ion heating is mainly caused via dissipation of the Alfvén mode via cyclotron resonance although fast modes can also contribute to perpendicular ion heating via the same mechanism. Slow modes dissipate via Landau resonance at the fluid scale, leading to parallel ion heating for low $\beta_p$. These are several pathways that density fluctuations can be connected to heating and dissipation. Density fluctuations can originate from either (or both) MHD waves or nonlinear structures, thus connecting the properties of density fluctuations to the strength of compressibility through two potentially distinct frameworks.

Fu et al. (2022) investigated the relationship between the rms density fluctuation amplitude $\langle \delta n_p^2 \rangle^{1/2} / \langle n_p \rangle = \delta n_{p_{\rm rms}} / \langle n_p \rangle$ and $M_t$ by performing a series of compressible 3D MHD simulations. They found a linear scaling, such that $\delta n_{p_{\rm rms}} / \langle n_p \rangle = \alpha M_t$. They find that this coefficient of proportionality $\alpha$ is dependent on cross helicity $\sigma_c = \frac{\langle z_+^2 \rangle - \langle z_-^2 \rangle}{\langle z_+^2 \rangle + \langle z_-^2 \rangle}$, and proton beta $\beta_p$, where $z_\pm = |\delta \boldsymbol{v} \pm \boldsymbol{b}_{\rm A}|$ are the Elsässer variables, $\delta \boldsymbol{v}$ is the fluctuating velocity vector of the solar wind, and $\boldsymbol{b}_{\rm A} = \boldsymbol{b}/\sqrt{4\pi m_p n_p}$ is the fluctuating magnetic field vector ($\boldsymbol{b}$)in Alfvén units. Similar scaling studies of solar wind density fluctuations have been carried out previously (e.g., Matthaeus et al. 1990; Tu & Marsch 1994; Adhikari et al. 2020b).

In the present study, we find that the scaling of normalized density fluctuations in the solar wind during PSP's perihelia (see Section 2 for data description and methods; see Figure 1 for overview of radial trends) varies nearly linearly with $M_t$ (see Figure 2). We also condition the results based on $\beta$ and $\sigma_c$ and compare with recent simulations showcasing behavior that is similarly observed (see Figure 3). However, we also find that a larger ensemble average of the same quantities yield different scaling properties. These results are expressed in Section 3. In Section 4, we review our results and discuss their impact on compressibility studies.

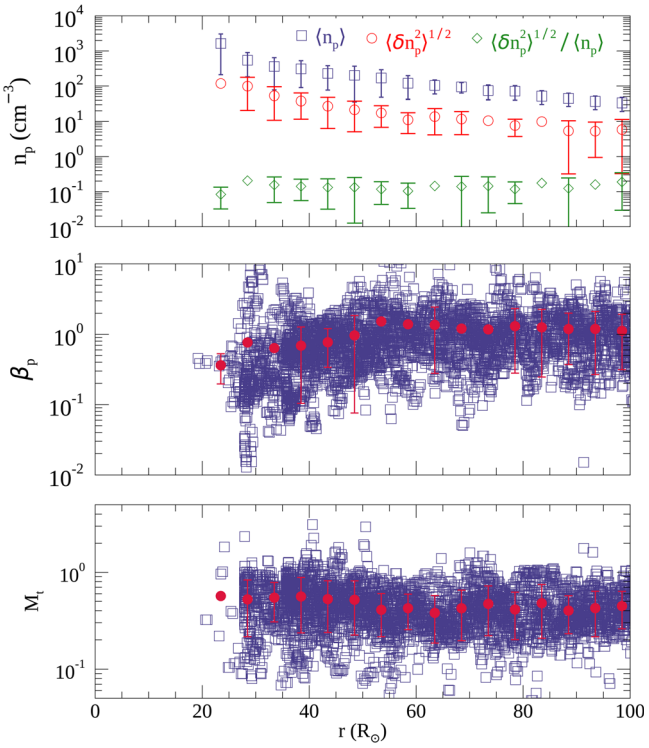


**Figure 1.** Overview of PSP observations in the inner heliosphere. Top: mean proton density $\langle n_p \rangle$, rms density fluctuation $\delta n_{p_{\rm rms}}$, and the ratio $\delta n_{p_{\rm rms}} / \langle n_p \rangle$ plotted as a function of heliocentric distance $r$. Data are aggregated from first eight PSP orbits and averaged within radial bins of size 5 $R_\odot$. Middle: proton plasma beta $\beta_{\rm p}$ aggregated from first eight PSP orbits (squares) and mean values (filled red circles) within radial bins of size 5 $R_\odot$. Bottom: turbulent Mach number $M_{\rm t} = \delta v / c_{\rm s}$ aggregated from first eight PSP orbits (squares) and mean values (filled red circles) within radial bins of size 5 $R_\odot$. Vertical bars represent standard deviation about corresponding means within the 5 $R_\odot$ bins. Note that error bars that extend to negative values are not shown on logarithmic axes. Only radial bins with at least ten counts are included. Note that we focus on $r \lesssim 50\ R_\odot$ in our main analysis (Section 3).

## 2. Parker Solar Probe Data

We use publicly available data[6] from the first eight orbits of PSP, covering the time period between 2018 October and 2021 June. Plasma data are from the Solar Probe Cup (SPC) on the SWEAP suite (Kasper et al. 2016; Case et al. 2020). For all orbits, we discard SPC data when the "general_flag" variable is on. Level 3 SPC moment data (see Case et al. 2020) are resampled to 1 s cadence using a linear interpolation. These data are then cleaned using a Hampel filter (Pearson 2002; Bandyopadhyay et al. 2018; Parashar et al. 2020) in the time domain, with a filtering interval of 120 s. Outliers are identified as values beyond 3 times the local standard deviation larger than the filtering interval's median. The outlier values are then replaced with the local median value.

To show the overall trend of density fluctuations from orbits 1 through 8, we smooth the 1 s cadence time series of $n_p$ using a boxcar average over a moving window of 2 hr duration to obtain the mean density $\langle n_p \rangle_{\rm 2hr}$ (at 1 s cadence), denoted by the following: $\langle \cdot \rangle_{\rm 2hr}$. The fluctuations in $n_p$ are then computed as $\delta n_p = n_p - \langle n_p \rangle_{\rm 2hr}$, from which we compute the rms density fluctuations $\langle \delta n_p^2 \rangle_{\rm 2hr}^{1/2}$ at 1 s cadence. Both $\langle n_p \rangle_{\rm 2hr}$ and $\langle \delta n_p^2 \rangle_{\rm 2hr}^{1/2}$ are then downsampled to 1 hr cadence.

[6] Obtained from the NASA Space Physics Data Facility.

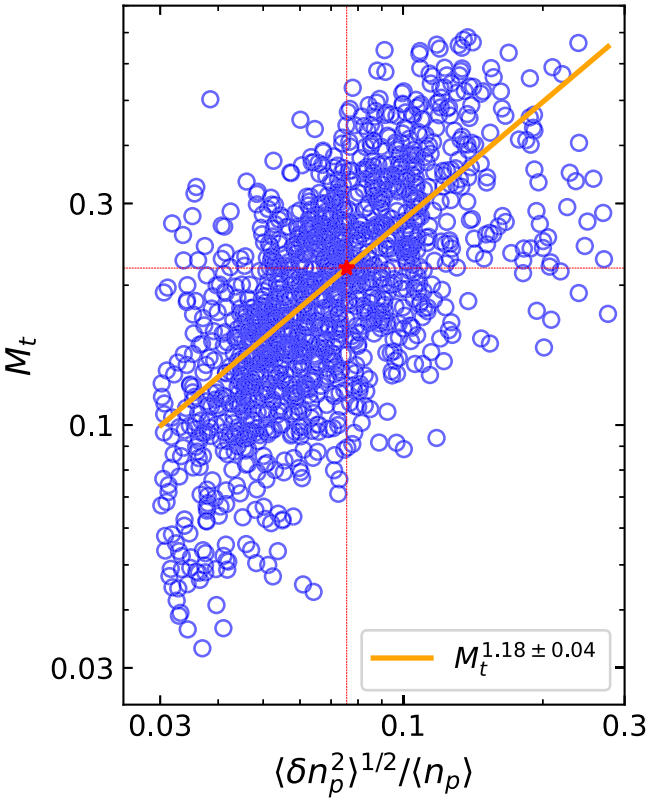


**Figure 2.** Compiled averages of $\delta n_{p_{\rm rms}}/\langle n_p \rangle$ and $M_t$ spanning 9 days for encounters 1–8. Blue circles represent 5 minute averages over nonoverlapping intervals wherein statistical quantities are computed via 5 minute rolling averages (see Section 2 for specifics on averaging techniques). A fitted power law is given by the solid orange line and is equivalent to $\delta n_{p_{\rm rms}}/\langle n_p \rangle \sim M_t^{1.18 \pm 0.04}$. The red star represents the average of $\delta n_{p_{\rm rms}}/\langle n_p \rangle$ and $M_t$ over all intervals.

An overview of the density profile for all eight orbits is shown in Figure 1, with radially binned statistics of size $5\,R_\odot$. As expected, the average proton density is increasing with decreasing heliocentric distance. The rms density fluctuation amplitude is also almost steadily increasing moving inwards. However, the normalized rms density fluctuation remains rather steady, except that it dips to lower values precipitously near $25\,R_\odot$. This might be an artifact of low sampling at these distances, requiring a larger available sampling from future PSP encounters. Changing this radial bin size to 10 and $2\,R_\odot$ produces no change in the trends.

We also provide overview trends of $\beta_p$ and $M_t$ in Figure 1, computed using a 2 hr averaging window with radial binning as described above. The turbulent Mach number ranges widely between 0.1 and 1, with averages around 0.5 and no significant trend with radial distance. From $100\,R_\odot$ inward, the proton beta stays near 1 until about $60\,R_\odot$, after which it decreases to an average of 0.3. The collection of these trends points toward identification of a heliocentric region $R < 50\,R_\odot$ ($\sim 0.25$ au) that may be meaningfully viewed as a low $\beta_p$ and intermediate $M_t$ environment. Therefore, we focus on distances in this range for the results below.

We now describe the averaging procedure used to obtain the results presented in Section 3; we start with the data resampled to 1 s cadence for the fundamental quantities $n_p$, $\boldsymbol{v}$, and $\boldsymbol{B}$. Fluctuations of these fundamental quantities are defined as $\delta n_p = n_p - \langle n_p \rangle_1$, $\delta \boldsymbol{v} = \boldsymbol{v} - \langle \boldsymbol{v} \rangle_1$, and $\boldsymbol{b} = \boldsymbol{B} - \langle \boldsymbol{B} \rangle_1$, where $\langle \cdot \rangle_1$ represents a 5 minute centered rolling average, with the averaging duration chosen to approximately match the correlation time of magnetic fluctuations observed during PSP's first several perihelia (e.g., Chen et al. 2020; Chhiber et al. 2021). Therefore, each fluctuating quantity is a time series with 1 s cadence. We then divide these quantities into nonoverlapping 5 minute subintervals, which are used to compute a final averaged value for these quantities within each subinterval, denoted as $\langle \cdot \rangle_2$. This gives the notation $\langle \cdot \rangle = \langle \langle \cdot \rangle_1 \rangle_2$. Finally, averages of these quantities over all nonoverlapping subintervals will be denoted by an overbar $\bar{\cdot}$. Unless otherwise specified, from here onward, $M_t$, $\beta_p$, and $\sigma_c$ refer to results obtained after the averaging procedure $\langle \cdot \rangle$ is performed. Note that $c_s$ can be computed from the proton thermal speed $\omega_p$ as $c_s \equiv \sqrt{5/3}\,\omega_p$, which can also be used in the framework of computing $M_t$ and to extract a temperature (or thermal pressure). Note that for this study, we assume that the temperature and density are equivalent for both the protons and electrons.

## 3. Results from Encounters 1–8

In this study, we examine the effects of $\sigma_c$ and $\beta_p$ on the relationship between $\delta n_{p_{\rm rms}}/\langle n_p \rangle$ and $M_t$. The interest here is in statistical characterization of beta, Mach number, and density fluctuations of the turbulence at the energy-containing scales. (Note that the inertial range, and its properties such as the spectrum, are separate issues not investigated here.) Therefore, we average the higher resolution samples over a time value on the order of the correlation time (5 minutes) at these radial distances. To achieve this balance between statistical significance and regional variation, please refer to Section 2 for averaging techniques.

Nine days from each encounter, centered around perihelion, are used, corresponding to a range of heliocentric distances $0.074 < R < 0.234$ au. Parameter ranges for the full set of data points are as follows: $\langle n_p \rangle \in [53,\ 1490.5]\,\mathrm{cm}^{-3}$ with a mean $\overline{\langle n_p \rangle} = 334\,\mathrm{cm}^{-3}$, $M_t \in [0.016,\ 1.31]$ with $\overline{M_t} = 0.211$, $\sigma_c \in [0.001,\ 0.962]$ with $\overline{\sigma_c} = 0.497$, and $\beta_p \in [0.048,\ 18.1]$ with $\overline{\beta_p} = 0.836$.

### 3.1. On the Scaling of Density Fluctuations with $M_t$

We investigate a possible power-law relationship between $\delta n_{p_{\rm rms}}/\langle n_p \rangle$ and $M_t$. Evaluating the standard errors in computing these two quantities ($\sigma_{\delta n_{p_{\rm rms}}/\langle n_p \rangle}$ & $\sigma_{M_t}$), we find that $\sigma_{\delta n_{p_{\rm rms}}/\langle n_p \rangle} \sim \sigma_{M_t}/10$ due to the propagation of error for $\delta n_{p_{\rm rms}}/\langle n_p \rangle$. We have also adjusted the nonoverlapping interval duration up to 120 minutes and experienced insignificant alterations of the results presented here, other than a decrease in the number of available samples. Based on these statistical considerations, we provide the power-law fit of $M_t$ as a function of $\delta n_{p_{\rm rms}}/\langle n_p \rangle$ and invert this relation to find an estimated scaling of the density fluctuations with respect to $M_t$. The reason for this lies within the power-law fitting method, which assumes that any error is introduced by the values of the function and not its dependent variable(s).

An overview of $M_t$ as a function of $\delta n_{p_{\rm rms}}/\langle n_p \rangle$ is shown in Figure 2. In this locally averaged point of view, we observe that $\delta n_{p_{\rm rms}}/\langle n_p \rangle \sim M_t^{1.18 \pm 0.04}$ as determined from the fit shown in Figure 2. This power law is close to the $M_t^{0.97}$ scaling observed by Adhikari et al. (2020b) in PSP's first orbit. Note that we have applied constraints on our analysis, such that intervals with values of $\delta n_{p_{\rm rms}}/\langle n_p \rangle < 0.03$ have been discarded due to

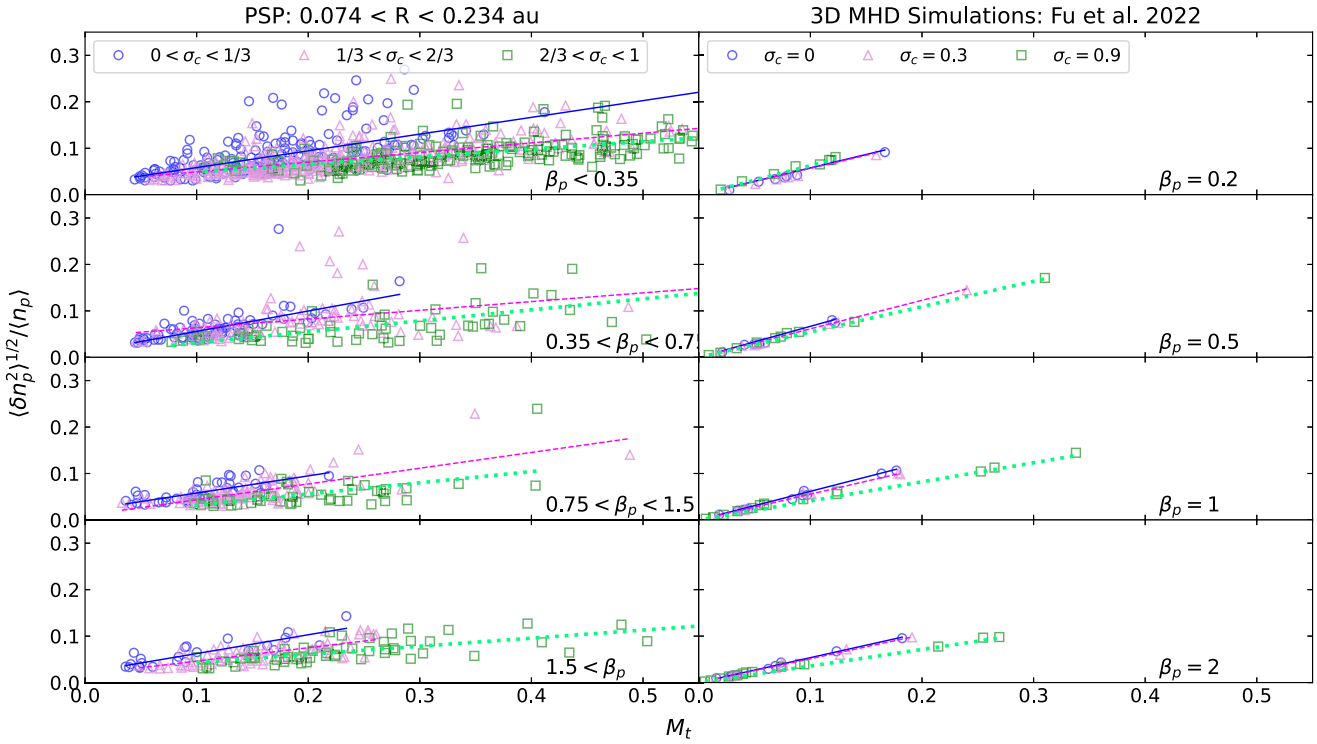


**Figure 3.** (Left column) Compiled averages of density fluctuations $\delta n_{p_{\rm rms}}/\langle n_p\rangle$ as a function of turbulent Mach number $M_t$ spanning 9 days each for PSP encounters 1–8. Points represent 5 minute averages over nonoverlapping intervals whose quantities are computed via 5 minute rolling averages (see Section 2 for specifics on averaging techniques). (Right column) $\delta n_{p_{\rm rms}}/\langle n_p\rangle$ as a function of $M_t$ for individual simulations, adapted from Fu et al. (2022). Both the left and right plots are conditioned on ranges of cross helicity $\sigma_c$ and proton plasma beta $\beta_p$. Solid blue, dashed pink, and dotted green lines represent fits to blue circles, pink triangles, and green squares, respectively.

**Table 1**
Linear Fits and Standard Errors ($\alpha \pm \sigma_\alpha$)

| $\langle\delta n_p^2\rangle^{1/2}/\langle n_p\rangle \sim \alpha M_t$ | $\beta_p < 0.35$ | $0.35 < \beta_p < 0.75$ | $0.75 < \beta_p < 1.50$ | $1.50 < \beta_p$ |
|---|---|---|---|---|
| $0 < \lvert\sigma_c\rvert < 1/3$ | $0.36 \pm 0.03$ | $0.44 \pm 0.06$ | $0.37 \pm 0.05$ | $0.41 \pm 0.05$ |
| $1/3 < \lvert\sigma_c\rvert < 2/3$ | $0.21 \pm 0.01$ | $0.19 \pm 0.05$ | $0.34 \pm 0.03$ | $0.29 \pm 0.03$ |
| $2/3 < \lvert\sigma_c\rvert < 1$ | $0.16 \pm 0.01$ | $0.24 \pm 0.04$ | $0.24 \pm 0.05$ | $0.17 \pm 0.02$ |

**Note.** Corresponding to the lines in Figure 3, which are conditioned on cross helicity $\sigma_c$ (rows) and plasma beta $\beta$ (columns).

instrument noise considerations (Case et al. 2020). Additionally, 1% of the lower and upper values of $M_t$ have been discarded to remove possible outliers from the core results.

The obtained power-law scaling is inconsistent with that predicted from NI theory for homogeneous flows (density fluctuations scale with $M_t^2$). The result obtained here follows much more closely the elementary prediction from linear theory or NI theory with an inhomogeneous background field (density fluctuations scale with $M_t$). However, significant statistical variations are seen.

Shifting to a global perspective for the relationship of these quantities, we perform averaging over the full set of nonoverlapping subintervals (all blue circles in Figure 2). We find that $\overline{\delta n_{p_{\rm rms}}/\langle n_p\rangle}/\overline{M_t} \approx 0.36$ and $\overline{\delta n_{p_{\rm rms}}/\langle n_p\rangle}/\overline{M_t}^2 \approx 1.70$. Values of $\overline{\delta n_{p_{\rm rms}}/\langle n_p\rangle}$ and $\overline{M_t}$ are shown in Figure 2 represented by the red star. While no formal conclusion can be formed based on these constants of proportionality, their values might be seen as slightly favoring the homogeneous NI theory. Perhaps most likely is that we are observing some mixture of inhomogeneous NI $M_t$ scaling and homogeneous NI $M_t^2$ scaling.

### 3.2. Influence of Plasma Beta and Cross Helicity on the Scaling

We also have examined the linear dependence of density fluctuations when separately grouping intervals conditioned on values of the parameters $\sigma_c$ and $\beta_p$. Specifically we examine how these properties affect the scaling of $\delta n_{p_{\rm rms}}/\langle n_p\rangle$ with $M_t$. There may be some $\gamma$ dependence, which is difficult to define from the data (however, see Totten et al. 1995; Livadiotis 2018; Nicolaou et al. 2019, 2020). Therefore, we set $\gamma = 1.67$ for the entirety of this study, noting that any change to $\gamma$ will not change any qualitative remarks on the observed conditioned trends. We compare our results with similar analyses based on compressible 3D MHD turbulence simulations performed by Fu et al. (2022). This will provide potential confirmation of observed effects when $\beta_p$ and $\sigma_c$ are varied. These conditioned-in-situ (left panel) and simulation (right panel) results are given in Figure 3. Since the overall results are well fit by a linear relationship between density fluctuations and Mach number (Figure 2), we perform linear fits $\delta n_{p_{\rm rms}}/\langle n_p\rangle = \alpha M_t$, represented by the straight lines in the left panel of Figure 3, with details of the fits provided in Table 1. These conditioned results

provide observations of different systematic changes for different combined ranges of $\sigma_c$ and $\beta_p$.

Specific conclusions are

1. For fixed $\sigma_c$, we observe no significant trend of linear coefficient $\alpha$ with respect to $\beta_p$.
2. For fixed $\beta_p$, we observe a decreasing $\alpha$ with increasing $\sigma_c$.

The description of these trends can be confirmed numerically via the linear least-squares fit to the function $\delta n_{p_{\rm rms}}/\langle n_p\rangle \sim \alpha M_t$ in Table 1 and by comparing the value of $\alpha$ over different pairings of $\sigma_c$ and $\beta_p$. Further discussion of these trends can be found in Section 4.

Next, we compare these trends with results based on 3D MHD simulations of compressible turbulence published by Fu et al. (2022). These results utilized the high-performance code ATHENA++ (Stone et al. 2020) to solve the ideal compressible MHD equations within an elongated box domain with periodic boundary conditions. The system started from a uniform mass density and uniform background magnetic field with zero fluctuations. Plasma parameters are selected to represent typical solar wind conditions found within 1 au. Further details on the simulations may be found in Fu et al. (2022).

The aforementioned observed trends are also seen in simulations (Fu et al. 2022), in which several runs of different $M_t$ and $M_A$ are used to compute a density fluctuation amplitude over the simulation domain for fixed $\sigma_c$ and $\beta_p$. The results with $\gamma = 1.67$ from Fu et al. (2022) are shown in the right panel of Figure 3. Here we note two caveats when comparing PSP observations to these simulations. The first is that the PSP observations correspond to averaging at around the energy injection scale, whereas simulation results presented in Figure 3 are computed for scales in the inertial range, although including the energy injection scales do not affect these trends. Second, results from the 3D MHD simulations are produced by global averaging over a 3D volume. Such averaging is not equivalent to spacecraft sampling along a 1D trajectory, which contains more random variations and may have a dependence on the angle between the sample trajectory and background magnetic field due to anisotropy of fluctuations (Du et al. 2023). A systematic bias can be introduced since PSP favors sampling of the solar wind parallel to the background magnetic field. However, since sampling likely affects the calculation of both $M_t$ and $\delta n_{p_{\rm rms}}/\langle n_p\rangle$ similarly, we expect the qualitative trends in the scaling relation to remain consistent even if proper directional averaging is made.

## 4. Discussion

We have examined the relationship between the normalized proton density variation and the turbulent Mach number, a problem that has been examined previously using several different spacecraft (Matthaeus et al. 1990; Tu & Marsch 1994) in different regions of the heliosphere, with Adhikari et al. (2020b) utilizing PSP's first encounter. Here we extend these studies to PSP's data set of the first eight encounters. We find a power-law scaling of $\delta n_{p_{\rm rms}}/\langle n_p\rangle \sim M_t^{1.18\pm0.04}$, consistent with NI theory extended to inhomogeneous background fields (Bhattacharjee et al. 1998; Hunana & Zank 2010), and also with the prediction based on linearized MHD equations. Since the best fit lies between the compressible wave scaling $\sim M_t$ and the NI scaling $\sim M_t^2$ expected for a homogeneous background field (Zank & Matthaeus 1993), it is also possible to interpret the observed result as representing a mixture of these two types of plasma states. We also examined the influence of the averaging domain on the relationship between density fluctuations and turbulent Mach number. When averaging over the full set of PSP intervals, we find that the coefficient of the $\sim M_t^2$ scaling is closer to unity than that of the $\sim M_t$ scaling, suggesting some relevance of the homogeneous NI theory.

Another interesting point of discussion is the relationship of the present results to both incompressive cascade rate laws (Politano & Pouquet 1998) and compressive cascade rate laws (Hadid et al. 2017). The empirical scaling found in the present paper may provide guidance as to which of these formulations may be most appropriate for application to the solar wind. Moreover, analyses that employ the compressive cascade rate formalism, such as Hadid et al. (2017) infer an empirical relationship between cascade rate and turbulent Mach number, i.e., $\epsilon \sim M^{2.67}$ for slow wind and $\epsilon \sim M^{1.5}$ for fast wind. Using our result that $\delta\rho \sim M^{1.18}$, and assuming the results can be combined, one may deduce a relationship between $\delta\rho$ and $\epsilon$ that may be interesting for future investigation. The same observational treatment finds a scaling between Mach number and internal energy in an isothermal approximation, an approximation that may not be optimal for the solar wind. Future studies might employ the present empirical results to delve more deeply into various forms of NI theory and cascade laws to provide additional constraints on the underlying theory. Such considerations are well beyond the present intended scope.

We also carry out a procedure similar to Fu et al. (2022) to examine the effects of plasma beta and cross helicity on the linear dependence of density fluctuations on $M_t$ and compare our observational analysis with their results from 3D MHD simulations (see Figure 3). From the conditioned results using PSP observations and in comparison to their simulation results, we find a consistency in the trends with increasing $\sigma_c$ for a given range of $\beta_p$ (see Table 1). One clear result is that when cross helicity is increased, the normalized density fluctuations are decreased. This is generally consistent with the idea that Alfvénic fluctuations are incompressive. It is rather significant that PSP observations in the compressible solar wind reflects the same systematic changes observed in compressible 3D MHD simulations.

One might want to develop a special treatment of density fluctuations for regions of solar wind having low plasma beta ($\ll 1$), a condition that occurs sometimes, especially in magnetic clouds (Smith et al. 2006) but is not common in general. Low plasma beta has been recently treated using weak turbulence theory based on fast magnetosonic modes (Galtier 2023). However, the absence of Alfvén modes in that treatment makes it unlikely to explain the observations in the present paper. Given that Alfvénic fluctuations are typically present (Chen et al. 2020), a relevant theory related to the generation of density fluctuations is the parametric decay instability (e.g., Fu et al. 2018) of Alfvén waves. However, this mechanism becomes more important at low plasma beta when the fluctuation is coherent, which, again, is not typical for the observations we have presented.

Anisotropy in the inner heliosphere due to a more dominantly radial magnetic field has been found to affect many properties of turbulence, such as differences in magnetic power spectra, correlation lengths, and heating when decomposing these quantities into parallel and perpendicular

components. A possible influence on the observed distributions and associated scalings is that these intervals are largely dominated by parallel sampling by PSP (Cuesta et al. 2022). Anisotropy can cause density fluctuations sampled along the mean magnetic field to be weaker compared to the fluctuations sampled transverse to the mean field (Du et al. 2023). Further analysis along the lines of prior investigations (e.g., Matthaeus et al. 1990; Zank et al. 1990; Matthaeus et al. 1996; Dasso et al. 2005) would be required to examine further the relationship between the well-studied types of anisotropy and the corresponding observed properties of the density fluctuations (V. Wang et al. 2023, in preparation). Another point of interest is to investigate these results in regards to solar wind speed. Although future PSP orbits may encounter more frequent, faster solar wind speeds, the intervals in this study favor slow wind speeds ($<450\,\mathrm{km\,s^{-1}}$) by nearly 98%.

This research is partially supported by NASA under the Heliophysics Supporting Research program grants 80NSSC18K1210 and 80NSSC18K1648, by the Parker Solar Probe Guest Investigator program 80NSSC21K1765 at the University of Delaware, by Heliophysics Guest Investigator program 80NSSC19K0284, and the PUNCH project under subcontract NASA/SWRI N99054DS. In collaboration with Los Alamos National Laboratory (LANL), and partially supported by a NASA LWS grant 80NSSC20K0377(subcontract 655-001), those affiliated with University of Delaware visited LANL in summer 2022 to work on this project. S.D. and H.L. acknowledge the support by DOE OFES program and LANL/LDRD program. Z.G. and X.F. are supported by NASA under Award No. 80NSSC20K0377.

## ORCID iDs

Manuel Enrique Cuesta https://orcid.org/0000-0002-7341-2992
Rohit Chhiber https://orcid.org/0000-0002-7174-6948
Xiangrong Fu https://orcid.org/0000-0002-4305-6624
Senbei Du https://orcid.org/0000-0003-1134-3909
Yan Yang https://orcid.org/0000-0003-2965-7906
Francesco Pecora https://orcid.org/0000-0003-4168-590X
William H. Matthaeus https://orcid.org/0000-0001-7224-6024
Hui Li https://orcid.org/0000-0003-3556-6568
John Steinberg https://orcid.org/0000-0003-2491-1661
Fan Guo https://orcid.org/0000-0003-4315-3755
Zhaoming Gan https://orcid.org/0000-0003-3886-0383
Emma Conrad https://orcid.org/0000-0002-3408-4754
Diana Swanson https://orcid.org/0000-0001-7496-9832

## References

Adhikari, L., Zank, G. P., & Zhao, L. L. 2020a, ApJ, 901, 102
Adhikari, L., Zank, G. P., Zhao, L. L., et al. 2020b, ApJS, 246, 38
Bandyopadhyay, R., Chasapis, A., Chhiber, R., et al. 2018, ApJ, 866, 81
Bavassano, B., & Bruno, R. 1995, JGR, 100, 9475
Bayly, B. J., Levermore, C. D., & Passot, T. 1992, PhFl, 4, 945
Bhattacharjee, A., Ng, C. S., & Spangler, S. R. 1998, ApJ, 494, 409
Case, A. W., Kasper, J. C., Stevens, M. L., et al. 2020, ApJS, 246, 43
Chen, C. H. K., Bale, S. D., Bonnell, J. W., et al. 2020, ApJS, 246, 53
Chhiber, R., Usmanov, A. V., Matthaeus, W. H., & Goldstein, M. L. 2021, ApJ, 923, 89
Chhiber, R., Usmanov, A. V., Matthaeus, W. H., Parashar, T. N., & Goldstein, M. L. 2019, ApJS, 242, 12
Cho, J., & Lazarian, A. 2003, MNRAS, 345, 325
Cuesta, M. E., Chhiber, R., Roy, S., et al. 2022, ApJL, 932, L11
Dasso, S., Milano, L. J., Matthaeus, W. H., & Smith, C. W. 2005, ApJL, 635, L181
Du, S., Li, H., Gan, Z., & Fu, X. 2023, ApJ, 946, 74
Fu, X., Li, H., Gan, Z., Du, S., & Steinberg, J. 2022, ApJ, 936, 127
Fu, X., Li, H., Guo, F., Li, X., & Roytershteyn, V. 2018, ApJ, 855, 139
Galtier, S. 2023, JPlPh, 89, 905890205
Gan, Z., Li, H., Fu, X., & Du, S. 2022, ApJ, 926, 222
Grappin, R., Mangeney, A., & Marsch, E. 1990, JGR, 95, 8197
Hadid, L., Sahraoui, F., & Galtier, S. 2017, ApJ, 838, 9
Hunana, P., & Zank, G. P. 2010, ApJ, 718, 148
Kasper, J. C., Abiad, R., Austin, G., et al. 2016, SSRv, 204, 131
Kasper, J. C., Klein, K. G., Lichko, E., et al. 2021, PhRvL, 127, 255101
Klein, L., Bruno, R., Bavassano, B., & Rosenbauer, H. 1993, JGR, 98, 7837
Kowal, G., Lazarian, A., & Beresnyak, A. 2007, ApJ, 658, 423
Livadiotis, G. 2018, Entrp, 20, 799
Makwana, K. D., & Yan, H. 2020, PhRvX, 10, 031021
Malara, F., Primavera, L., & Veltri, P. 1996, JGR, 101, 21597
Matthaeus, W. H., & Brown, M. R. 1988, PhFl, 31, 3634
Matthaeus, W. H., Ghosh, S., Oughton, S., & Roberts, D. A. 1996, JGR, 101, 7619
Matthaeus, W. H., Goldstein, M. L., & Roberts, D. A. 1990, JGR, 95, 20673
Matthaeus, W. H., Klein, L. W., Ghosh, S., & Brown, M. R. 1991, JGR, 96, 5421
Montgomery, D., Brown, M. R., & Matthaeus, W. H. 1987, JGR, 92, 282
Nicolaou, G., Livadiotis, G., & Wicks, R. T. 2019, Entrp, 21, 997
Nicolaou, G., Livadiotis, G., Wicks, R. T., Verscharen, D., & Maruca, B. A. 2020, ApJ, 901, 26
Parashar, T. N., Goldstein, M. L., Maruca, B. A., et al. 2020, ApJS, 246, 58
Pearson, R. K. 2002, IEEE Trans Control Syst Technol, 10, 55
Politano, H., & Pouquet, A. 1998, GeoRL, 25, 273
Roberts, D. A., Goldstein, M. L., & Klein, L. W. 1990, JGR, 95, 4203
Roberts, D. A., Goldstein, M. L., Klein, L. W., & Matthaeus, W. H. 1987a, JGR, 92, 12023
Roberts, D. A., Klein, L. W., Goldstein, M. L., & Matthaeus, W. H. 1987b, JGR, 92, 11021
Shoda, M., Suzuki, T. K., Asgari-Targhi, M., & Yokoyama, T. 2019, ApJL, 880, L2
Smith, C. W., Vasquez, B. J., & Hamilton, K. 2006, JGRA, 111, A09111
Stone, J. M., Tomida, K., White, C. J., & Felker, K. G. 2020, ApJS, 249, 4
Totten, T. L., Freeman, J. W., & Arya, S. 1995, JGR, 100, 13
Tu, C. Y., & Marsch, E. 1994, JGR, 99, 21,481
Yang, L. P., Li, H., Li, S. T., et al. 2019, MNRAS, 488, 859
Yang, Y., Matthaeus, W. H., Shi, Y., Wan, M., & Chen, S. 2017, PhFl, 29, 035105
Yang, Y., Shi, Y., Wan, M., Matthaeus, W. H., & Chen, S. 2016, PhRvE, 93, 061102
Yang, Y., Wan, M., Matthaeus, W. H., & Chen, S. 2021, JFM, 916, A4
Zank, G. P., Adhikari, L., Hunana, P., et al. 2017, ApJ, 835, 147
Zank, G. P., & Matthaeus, W. H. 1992, JPlPh, 48, 85
Zank, G. P., & Matthaeus, W. H. 1993, PhFl, 5, 257
Zank, G. P., Matthaeus, W. H., & Klein, L. W. 1990, GeoRL, 17, 1239
Zank, G. P., Zhao, L. L., Adhikari, L., et al. 2021, PhPl, 28, 080501